Journal of Molecular Graphics and Modelling 61 (2015) 21–29

Contents lists available at ScienceDirect

Journal of Molecular Graphics and Modelling

journal homepage: www.elsevier.com/locate/JMGM

Theoretical study of the hydrolysis mechanism of 2-pyrone-4,6-dicarboxylate (PDC) catalyzed by LigI

Shujun Zhang [a], Guangcai Ma [a], Yongjun Liu [a,b,*], Baoping Ling [c]

[a] School of Chemistry and Chemical Engineering, Shandong University, Jinan, Shandong 250100, China
[b] Key Laboratory of Tibetan Medicine Research, Northwest Institute of Plateau Biology, Chinese Academy of Sciences, Xining, Qinghai 810001, China
[c] School of Chemistry and Chemical Engineering, Qufu Normal University, Qufu, Shandong 273165, China

ARTICLE INFO

Article history:
Received 28 April 2015
Received in revised form 9 June 2015
Accepted 20 June 2015
Available online 25 June 2015

Keywords:
2-Pyrone-4,6-dicarboxylate lactonase
LigI
2-Pyrone-4,6-dicarboxylate (PDC)
QM/MM
Hydrolysis mechanism

ABSTRACT

2-Pyrone-4,6-dicarboxylate lactonase (LigI) is the first identified enzyme from amidohydrolase superfamily that does not require a divalent metal ion for catalytic activity. It catalyzes the reversible hydrolysis of 2-pyrone-4,6-dicarboxylate (PDC) to 4-oxalomesaconate (OMA) and 4-carboxy-2-hydroxymuconate (CHM) in the degradation of lignin. In this paper, a combined quantum mechanics and molecule mechanics (QM/MM) approach was employed to study the reaction mechanism of LigI from *Sphingomonas paucimobilis*. According to the results of our calculations, the whole catalytic reaction contains three elementary steps, including the nucleophilic attack, the cleavage of C—O of lactone (substrate) and the intramolecular proton transfer. The intermediate has two intramolecular proton transfer pathways, due to which, two final hydrolysis products can be obtained. The energy profile indicates that 4-carboxy-2-hydroxymuconate (CHM) is the main hydrolysis product, therefore, the isomerization between 4-carboxy-2-hydroxymuconate (CHM) and 4-oxalomesaconate (OMA) is suggested to occur in solvent. During the catalytic reaction, residue Asp248 acts as a general base to activate the hydrolytic water molecule. Although His31, His33 and His180 do not directly participate in the chemical process, they play assistant roles by forming electrostatic interactions with the substrate and its involved species in activating the carbonyl group of the substrate and stabilizing the intermediates and transition states.

1. Introduction

Lignin is a kind of complex aromatic heteropolymer found in nature whose main role in plants is to increase cell wall integrity and resistance to attack by pathogens. Lignin and its degradation products have potential applications in the production of biofuels and the manufacture of polyesters and adhesives [1–3]. Furthermore, the degradation of lignin contributes a lot in the carbon cycle [4]. Many enzymes are involved in the lignin degradation, for example, the lignin peroxidase (Lip) [5], the heme-containing manganese peroxidases (MnP) [6] and the versatile peroxidases (VP) [7]. The enzyme 2-pyrone-4,6-dicarboxylate lactonase (LigI) plays an important role in the metabolism of lignin-derived aromatic compounds [2,5,8], which catalyzes the reversible hydrolysis of 2-pyrone-4,6-dicarboxylate (PDC) to a mixture of 4-carboxy-2-hydroxymuconate (CHM) and 4-oxalomesaconate (OMA), as shown in Scheme 1 [2].

According to the amino acid sequence alignments, LigI belongs to the amidohydrolase superfamily (AHS), which catalyze a diverse set of chemical reactions, including the hydrolysis of amide or ester bonds, the deamination of nucleic acids, hydration, isomerization and decarboxylation [2,9,10]. Most of the AHS members contain one to three divalent metal ions in their active sites [11]. Generally, the divalent metal ions play significant role in activating a water molecule for nucleophilic attack on amide or ester bonds [12,13]. However, LigI does not have bound metal ions in its active site, and therefore, the active site is different from those of other members of amidohydrolase superfamily [2]. Hobbs et al. have experimentally proved that the addition of divalent metal ions to enzymatic assays have no help for enhancing its biological activity [2]. To explore the catalytic mechanism of LigI, the structures of the wild-type LigI from *Sphingomonas paucimobilis* [6,14–16], and the site-directed mutant proteins, including D248A complexed with substrate (PDB code: 4DI8, pH 8.5, resolution 1.81 Å), D248A complexed with product (PDB code: 4DI9, pH 6.5, resolution 1.35 Å), and D248N complexed with neither substrate nor product (PDB

* Corresponding author at: School of Chemistry and Chemical Engineering, Shandong University, Jinan, Shandong 250100, China. Fax: +86 53188564464.
E-mail address: yongjunliu_1@sdu.edu.cn (Y. Liu).

http://dx.doi.org/10.1016/j.jmgm.2015.06.011
1093-3263/

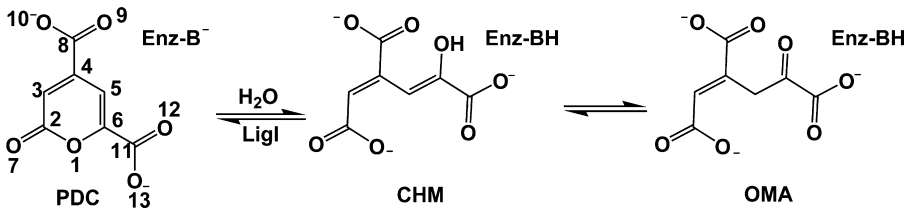

Scheme 1. Hydration catalyzed by LigI.

code: 4DIA, pH 4.6, resolution 2.00 Å) have been obtained, and the site-directed mutagenesis studies and pH-rate profiles have been performed. Based on these experimental results, Hobbs et al. proposed a two-step sequential mechanism for the catalysis of LigI [2]. In the first step, the hydrolytic water molecule is activated by an active site residue, simultaneously, the generated hydroxyl anion attacks on the substrate carbonyl, forming a tetrahedral intermediate. In the second step, the C2—O1 bond of lactone is cleaved, yielding the hydrolysis products. Through various mutants and kinetics analysis, the conserved Asp248 was suggested to act as the general base, and the carbonyl group of PDC is activated by electrostatic interactions with three conserved residues His31, His33 and His180. Their experimental data also proved that OMA is the predominant product at pH 10, and CHM is the main product at pH 6.

Although a rough picture of the catalytic mechanism of LigI has been obtained, the reaction detail is still unknown. For example, the hydrolysis products of the reaction exist in two forms at pH value from 8 to 9 [2]. Are they produced by enol-to-keto tautomerization in solvent or both of them can be directly generated in the active site by the hydrolysis of substrate? Which step determines the whole reaction rate and how the key residues influence the reaction barrier? These questions cannot be acquired by experiments alone. Therefore, in the present work, the catalytic mechanism of LigI was further studied by using a combined quantum mechanics and molecule mechanics (QM/MM) method, which has been successfully applied in exploring the enzymatic mechanism in the past years [17–24]. Based on the results of our calculations, the energetic details of the whole reaction cycle have been given, the structures of the reactant and its involved species, and the roles of key residues have been delineated at atomistic level. To our knowledge, this is the first time for the reaction mechanism of 2-pyrone-4,6-dicarboxylate lactonase (LigI) to be studied from theoretical aspect.

2. Computational methods

2.1. Model preparation

Construction of the enzyme-substrate complex is the requisite for theoretical investigation of an enzymatic reaction. It is generally difficult to crystallize a structure of an enzyme-substrate complex by experimental method under regular condition because the enzyme-substrate complex usually converts directly to the enzyme-product complex. Therefore, our computational model was constructed from the crystal structure of a site-directed mutant D248A (PDB code: 4DI8, resolution 1.81 Å), which was actually a complex of mutanted enzyme with the substrate (PDC). To construct the reactant model, the mutanted residue Ala248 was manually mutated back to Asp248 with the VMD program [25]. The protonation states of charged residues were assigned on the basis of their pKa values determined by the empirical PROPKA program [26], and then their individual local hydrogen bonds were inspected with the visual software VMD [25]. The calculation results indicate that aspartic acid (Asp248) is negatively charged and the two arginines (Arg130 and Arg124) are positively charged in the active site, while the initial protonation states of His31, His33, and His180 are singly protonated on ϵ sites, which agree well with the previous investigation [2]. All missing hydrogen atoms were added by means of the HBUILD module in the CHARMM program package [27]. The force field parameters and atomic charges of the substrate were constructed according to the structurally similar molecules that have been parameterized in the force field, which are shown in Table S1 of Supporting information.

The prepared structure was then surrounded by a TIP3P water droplet with 30 Å radius while all crystal water molecules were preserved, and further neutralized by addition of sodium ions at random positions. Finally, the resulting system consists of 13,526 atoms in total, including 294 residues, substrate, 2975 TIP3P water molecules and 14 sodium ions. The prepared system was firstly equilibrated by a series of energy minimizations and a 7 ns MD simulation were carried out by enforcing the stochastic boundary condition [43] at 298 K and 1 atm, which acts as a thermal bath to avoid the escape of water molecules from the dynamic region and keep the stability of the system. The MD simulation was performed by using the CHARMM22/CMAP all-atom force field [28] module implemented in the CHARMM program [27]. During the last 3 ns MD simulation, the trajectory tends to be flat, as shown in the Supporting Information (Fig. S1), which indicates that the system was basically equilibrated and the last snapshot from the MD trajectories was employed for the following QM/MM calculations.

2.2. QM/MM calculations

After the enzyme-substrate complex was constructed and equilibrated using the CHARMM22 force field [28], the system was partitioned into QM and MM subsystems. The QM subsystem contains 113 atoms, including the side chains of Asp248, His180, His33, His31, Arg124, Tyr49, Arg130, Tyr156, substrate, and a water molecule, as illustrated in Fig. S2 of Supporting information. All the remaining atoms of the system were assigned to the MM subsystem. The total charge of QM subsystem is −1 and the spin multiplicity is 1. All QM atoms and MM atoms within a distance of 15 Å from C2 of the substrate were kept active during the geometrical optimization, whereas all the remaining atoms were kept frozen to decrease the energy fluctuation and to reduce the CPU requirements. All QM/MM calculations were carried out using the ChemShell program suite [29]. The QM subsystem was treated by hybridized density functional theory method (B3LYP) with 6–31G (d, p) basis set using the TURBOMOLE software [30], and the MM subsystem was treated by CHARMM22 force field implemented in the DL-POLY program [31]. The electrostatic interactions between the QM and MM subsystems were described by the electronic embedding scheme [32] which incorporates the MM charges into the one-electron Hamiltonian of the QM calculation to avoid the hyperpolarization of the QM wave function. The interactions between the MM and the QM/MM were described by the no electrostatic cutoff model. To saturate the valence at the QM/MM boundaries, the link atom approach with a charge shift method was employed [33,34].

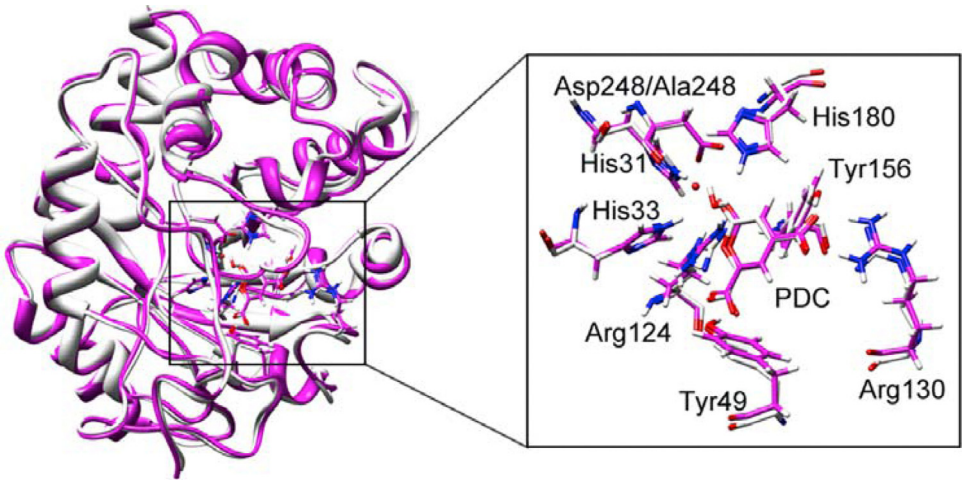

Fig. 1. The superposition of the crystal structure of D248A (the ribbon and carbon atoms are colored in light grey) with the QM/MM optimized computational model (the ribbon and carbon atoms are colored in purple), in which the alanine residue has been mutated back to aspartic residue. The RMSD of the backbones of the two structures is 0.55 Å.(For interpretation of the references to color in this figure legend, the reader is referred to the web version of this article.)

During the QM/MM calculations, geometry optimizations were performed by the hybrid delocalized internal coordinates (HDLC) optimizers [27], and the minima were found by a Quasi-Newton limited memory Broyden–Fletcher–Goldfarb–Shanno (L-BFGS) method [35,36]. Starting from the optimized reactant geometry, the relaxed potential energy surface (PES) scans were firstly performed to study the reaction path, and each point of the scan was performed by the partitioned rational function optimization (P-RFO) algorithm [37,38] implemented in the HDLC code. During the reactions, the reaction coordinate was defined by a combination of bond distances that are directly involved in chemical bond cleavage or formation. The structure of the highest point on the energy profile along the reaction coordinate was taken as the first approximation of the transition state geometry, which was further optimized by using the P-RFO optimizer [37,38]. P-RFO method is a Hessian eigenmode-following algorithm for the search of transition state, and each transition state features a unique negative eigenvalue [44].

Based on the optimized geometries, high-level single-point energy calculations were performed using a larger basis set of B3LYP/6-31++G (d, p) [39]. Finally, to correct the B3LYP energies for dispersion, all energies were rectified by the dispersion correction of DFT-D3 [40,41].

3. Results and discussion

3.1. Structure of 2-pyrone-4,6-dicarboxylate lactonase (LigI)

As described above, the initial structure was firstly constructed from the crystal structure of site-directed mutant D248A (PDB code: 4DI8). Then, the system was subjected to a series of MD simulations and QM/MM optimization. For comparison, the superposition of the crystal structure of D248A with the QM/MM optimized reactant model is displayed in Fig. 1. One can see that the two structures are visually superimposed well. The root-mean-square deviation (RMSD) of the backbones of the two structures was calculated to be 0.55 Å, and the pocket residues superimpose well, further indicating that the replacement of aspartic residue by alanine and the subsequent optimizations did not cause a larger conformational change.

As displayed in Fig. 2, in the active pocket of the reactant, PDC is stabilized by forming a complex hydrogen bond network with the side chains of the pocket residues. Arg124 forms two strong hydrogen bonds and one rather weak one with O7, O13 and O1 of the substrate with distances of 1.87 Å, 1.89 Å and 2.56 Å, respectively. Arg130 forms two strong hydrogen bonds with the carboxyl O9 and O10 with distances of 1.78 Å and 1.83 Å, respectively. In addition, the hydrolytic water molecule is fixed by two strong hydrogen bonds formed by Asp248 and His33 with distances of 1.56 Å and 1.85 Å, respectively. His31and His180 also lie hydrogen bond distances of 2.70 Å and 1.89 Å to the carbonyl O7. On the whole, the pocket residues and substrate form a complex hydrogen bond network.

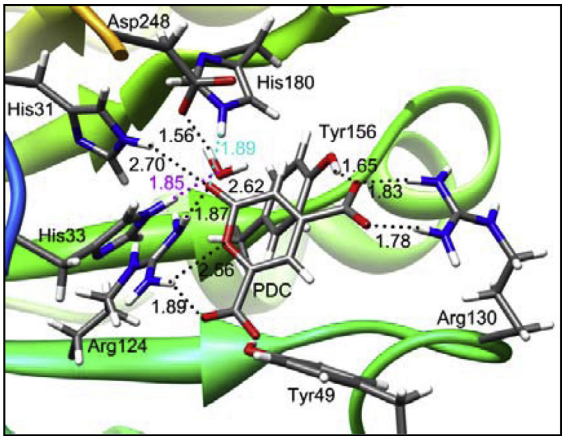

Fig. 2. QM/MM optimized active site structure of reactant (PDB code: 4DI8). Distances are shown in Å.

3.2. Calculated reaction mechanism

According to the earlier proposal [2] and our calculations, the total catalytic cycle can be divided into three distinct chemical steps, as outlined in Scheme 2. The first step corresponds to a nucleophilic attack, in which the deprotonated carboxyl group of Asp248 acts as a general base to activate the hydrolytic water molecule, and simultaneously, the generated hydroxyl anion attacks on the carbonyl group of PDC, forming a tetrahedral intermediate (IM1). Then, the C—O bond of PDC is broken to generate IM2. In IM2, there are two pathways for intramolecular proton transfer, corresponding to two final products (CHM and OMA). The optimized reactant, transition states, intermediates and the products are shown in Figs. 3 and 4.

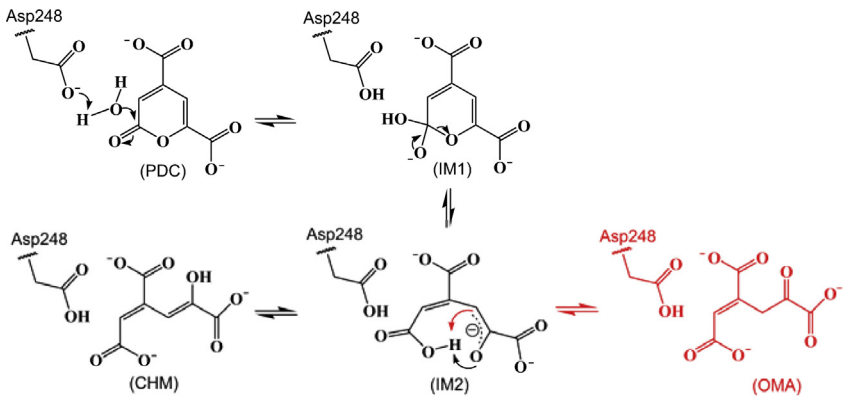

Scheme 2. Proposed mechanism of LigI based on our calculations and the reference [2].

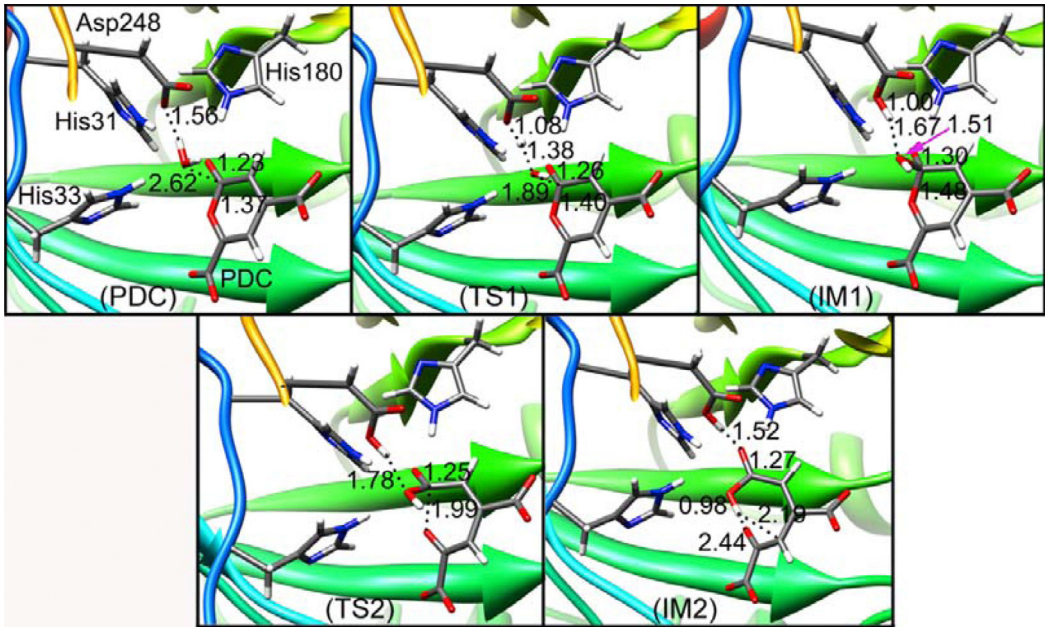

Fig. 3. Optimized structures of reactant (PDC), transition states (TS1, TS2), and intermediates (IM1, IM2) for the wild type enzyme. Distances are given in Å.

Based on the results of our calculation, in the first step, the activation of water molecule and the nucleophilic attack of hydroxyl anion on the carbonyl group of PDC proceed through a concerted mechanism. As shown in Fig. 3, in the reactant (PDC), the distance between the carboxyl oxygen atom of Asp248 and the hydrogen atom of hydrolytic water is 1.56 Å, and the distance between the C2 of PDC and the oxygen atom of the water molecule is 2.62 Å. By checking the structure of transition state TS1 shown in Fig. 3, one can see that the activation of hydrolytic water is prior to the nucleophilic attack of hydroxyl anion, which means the activation of the water molecule being the prerequisite for nucleophilic attack. The calculated energy barrier for the first step is 12.0 kcal/mol and the relative energy of intermediate IM1 is 7.2 kcal/mol, as shown in Fig. 5. The negatively charged tetrahedral intermediate (IM1) is stabilized by a strong hydrogen bond network formed by the intermediate and the side chains of Asp248, His180, His31, His33, and Arg124, as shown in Fig. S3 of Supporting information.

The second step corresponds to the cleavage of C2—O1 bond of the substrate, forming intermediate IM2. The optimized transition state (TS2) and intermediate (IM2) are shown in Fig. 3. In TS2, the length of C2—O1 bond increases from 1.48 Å to 1.99 Å. Downhill from the transition state TS2, the intermediate IM2 is generated with the complete broken of C2—O1 bond. The calculated energy barrier of this step is 7.1 kcal/mol, meaning the cleavage of C2—O1 bond being quite easy. In addition, the negatively charged O1 atom of the intermediate IM2 is also stabilized by a strong ion pair interaction with the guanidinium group of residue Arg124, as shown in Fig. S4 of Supporting information.

In the third step, the intramolecular proton transfer occurs in two different ways, generating two hydrolysis products. As shown in Scheme 2, the carboxyl proton of intermediate IM2 may transfer to C5 or O1 anion of the substrate, leading to the formation of OMA and CHM, respectively. The optimized transition states (TS3 and TS3′) and products (OMA and CHM) are displayed in Fig. 4.

From the structure of IM2, one can see that the proton to be transferred locates in a right position, which is only 2.19 Å far from C5. As shown in Fig. 5, the energy barrier for the formation of OMA is 6.7 kcal/mol. In addition, the proton can transfer more easily to the O1 anion, generating CHM, which corresponds to an even low energy barrier of 0.8 kcal/mol.

In summary, both of the two products can be directly obtained in the active site, but CHM is the main hydrolysis product. According to the experimentally obtained k_{cat} of 340 s^{-1} [2], the estimated free energy barrier is 14.2 kcal/mol, which agrees well with our calculation results. But we should realize that the calculated result was only derived from one snapshot of the MD simulations, thereby

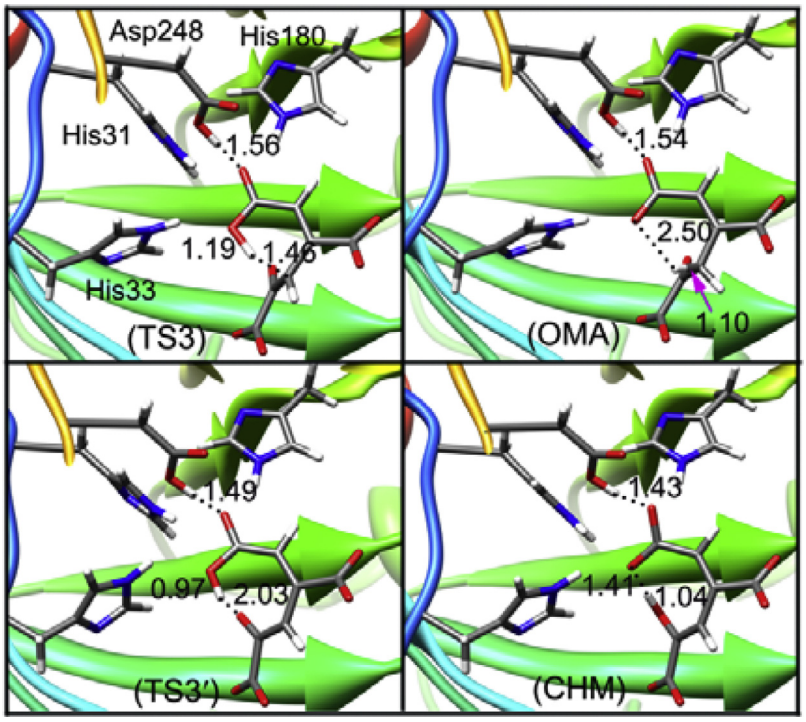

Fig. 4. Optimized structures of transition states (TS3, TS3′) and products (OMA, CHM) for the wild type enzyme. Distances are given in Å.

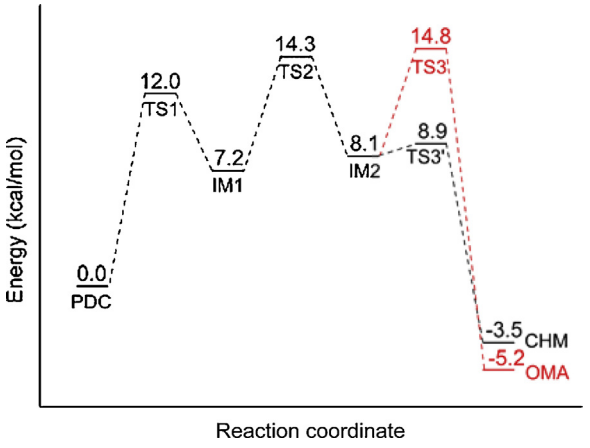

Fig. 5. Energy profile of PDC hydrolysis reaction catalyzed by LigI.

it is not conclusive considering the sampling of our QM/MM calculations. Besides, the present calculation results cannot give the pH dependence of the two forms of the product. Hobbs et al. have proved that the two forms of the hydrolysis products depend on the pH value [2], i.e., at pH 10, the keto form (OMA) was predominant, and at pH 6.0, the enol form (CHM) was predominant. Considering the transformation of the two forms of the products being very easy in solvent, we conjecture that it is the pH of the solvent that influences the equilibrium concentrations of OMA and CHM, but not the chemistry in the active site.

3.3. Analysis of three mutant residues

The mutation of His31 to Asn reduced k_{cat}/K_m by more than 4 orders of magnitude, while the mutation of either His33 to Asn, or His180 to Ala only reduces the kinetic constant by 2 orders of magnitude[2]. Although these mutagenesis experiments have provided much information, the detailed information about how residues His31, His33, and His180 influence the reaction is still unclear. To elucidate their roles in catalysis, we further performed QM/MM calculations on the basis of H31N, H33N and H180A mutants. Mutations were performed by VMD [25], then additional 3 ns MD simulation was carried out on each model using the CHARMM22 force field [28]. On the basis of the structures taken from the MD simulation, geometry optimizations were carried out using QM/MM method at the same level as for the wild type enzyme. There are few common characters in these three mutants: (1) each catalytic reaction proceeds through two elementary steps; (2) only the enol form (CHM) of the product was obtained in the active site; (3) the cleavage of C—O bond of the lactone was accompanied by the intramolecular proton transfer.

3.3.1. H31N mutant

Experimentally, the kinetic constant of H31N is 0.4 s^{-1}, which is much lower than that of the wild type enzyme (340 s^{-1}). Since His31 does not directly participate in the reaction, the great loss of catalytic power making the role of this residue more complicated. According to the experimental kinetic constant, the free energy barrier of H31N mutant is estimated to be 18.3 kcal/mol. Based on the active site structure shown in Fig. 2, His31 only forms a hydrogen bond with the carbonyl O7 of substrate with a distance of 2.70 Å. But in the active site of H31N mutant, no hydrogen bond is found between Asn31 and the substrate. Other residues keep similar interaction with the substrate, except an obvious structural change in the position of Arg124, as illustrated in Fig. S5 of Supporting information. The optimized reactant and its involved species are shown in Fig. 6.

On the basis of our calculation, the first step is similar to the wild type enzyme, also corresponding to the activation of the hydrolytic water molecule and the nucleophilic attack of hydroxyl anion on the carbonyl group of PDC. But this step has an energy barrier of 15.3 kcal/mol, which is higher than that of the wild type enzyme (12.0 kcal/mol). The second step corresponds to the cleavage of C2—O1 bond accompanied by an intramolecular proton transfer. In transition state (TS2-a), the length of C2—O1 bond changes

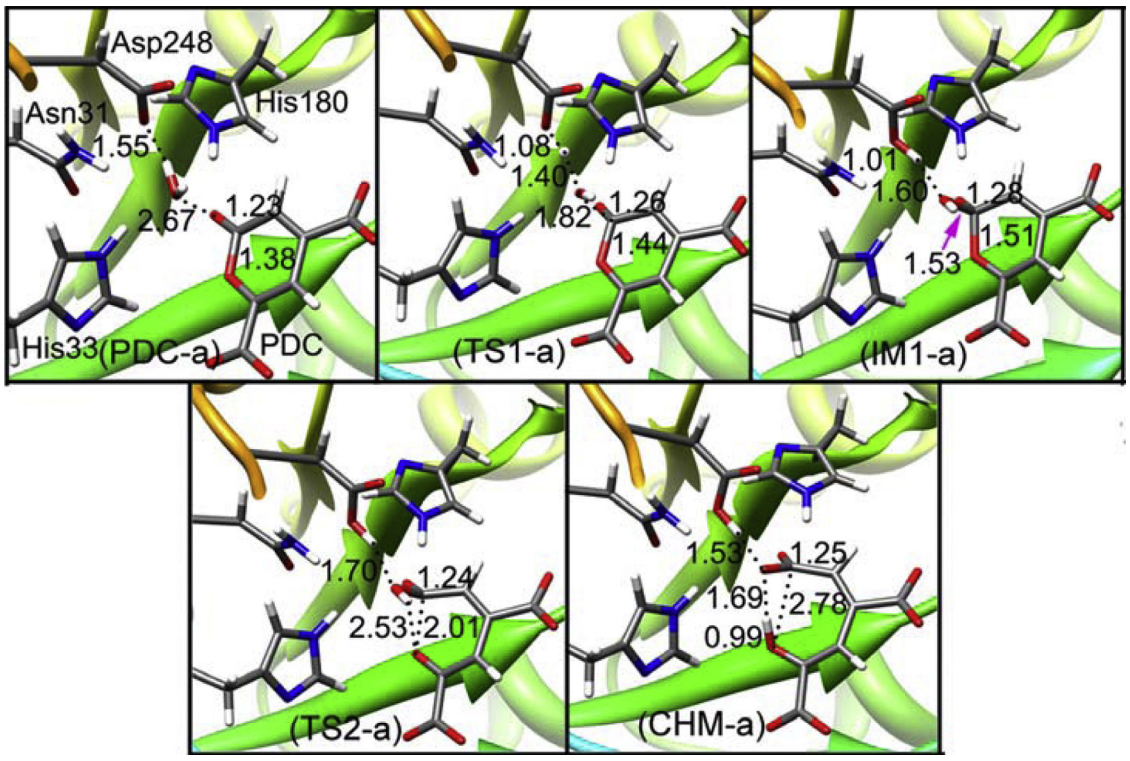

Fig. 6. Optimized geometries for H31N mutant. Distances are given in Å.

Table 1
The calculated relative energies of wild type enzyme and its three mutants (H31N, H33N and H180A). Energies are given in kcal/mol.

Enzyme	PDC	TS1	IM1	TS2	IM2	TS3′/TS3	CHM/OMA
Wild type	0.0	12.0	7.2	14.3	8.1	8.9/14.8	−3.5/−5.2
H31N	0.0	15.3	13.5	17.6			−1.1
H33N	0.0	16.7	9.6	14.1			4.0
H180A	0.0	13.7	11.9	13.7			−3.3

from 1.51 Å to 2.01 Å. Downhill from TS2-a, the enol form of the product (CHM-a) is directly generated with an energy barrier of 4.1 kcal/mol, in which the distance of C2—O1 increases from 2.01 Å to 2.78 Å. We also note that in TS2-a, the distance between the carboxyl proton at C2 and O1 is 2.53 Å, but it changes to 0.99 Å in the product, implying that the intramolecular proton transfer couples with the cleavage of C2—O1 bond. The overall energy barrier of H31N mutant is 17.6 kcal/mol, as shown in Table 1, which is approximately 3 kcal/mol higher than that of the wild type enzyme. This agrees well with the experimental results, further explaining the observation that mutation of His31 to Asn31 reduces the enzymatic activity.

Above information indicates that although residue His31 does not directly participate in the chemical reaction, it plays role in the stabilization of transition states and intermediates by electrostatic interaction. In addition, the high reduction in enzymatic activity of H31N mutant may also be assigned to the slight structural reorganization of the active pocket.

3.3.2. H33N mutant

The optimized geometries for H33N mutant are displayed in Fig. 7. Similar to H31N mutant, in the reactant, no hydrogen bond is formed between residue Asn33 and the hydrolytic water molecule, but in the wild type enzyme, His33 forms a strong hydrogen bond with this water molecule. In the reactant (PDC-b), the distance between the carboxyl oxygen of Asp248 and the hydrolytic water molecule is 1.69 Å, which is longer than that in the wild type enzyme. In addition, the distance between the water molecule and the C2 of PDC is also longer than that in the wild type enzyme (3.05 Å vs 2.62 Å). These two longer distances mean that the activation of the water molecule and the attack of generated hydroxyl anion on the C2 of PDC being more difficult. Just as expected, the calculated energy barrier of the first step is 16.7 kcal/mol. It is in consistent with the free energy barrier of 17.0 kcal/mol estimated from the k_{cat} of 3.6 s^{-1}, which is about 2 kcal/mol higher than that of the wild type enzyme. The relative energy of intermediate IM-b is 9.6 kcal/mol, which is higher than that of IM1 in the wild type enzyme. These results indirectly indicate that His33 plays a role in activating the hydrolytic water and stabilizing the intermediate IM1 by electrostatic interaction. For the second step, the H33N mutant is very similar to that of H31N, i.e., the cleavage of C2—O1 bond is accompanied by an intramolecular proton transfer with a lower energy barrier of 4.5 kcal/mol, generating the enol form of the product (CHM-b).

3.3.3. H180A mutant

As shown in Fig. 2, in the active site of reactant, residue His180 forms a hydrogen bond with O7 of the substrate. But after His180 is mutated to Ala180, this hydrogen bond no longer exists. The optimized geometries are given in Fig. 8. In the reactant (PDC-c), the positions of the hydrolytic water molecule and the substrate and Ala180 are similar to those of wild type enzyme. The distances from the water molecule to Asp248 and C2 of PDC are 1.61 Å and 2.71 Å, respectively, which are close to the values in the wild

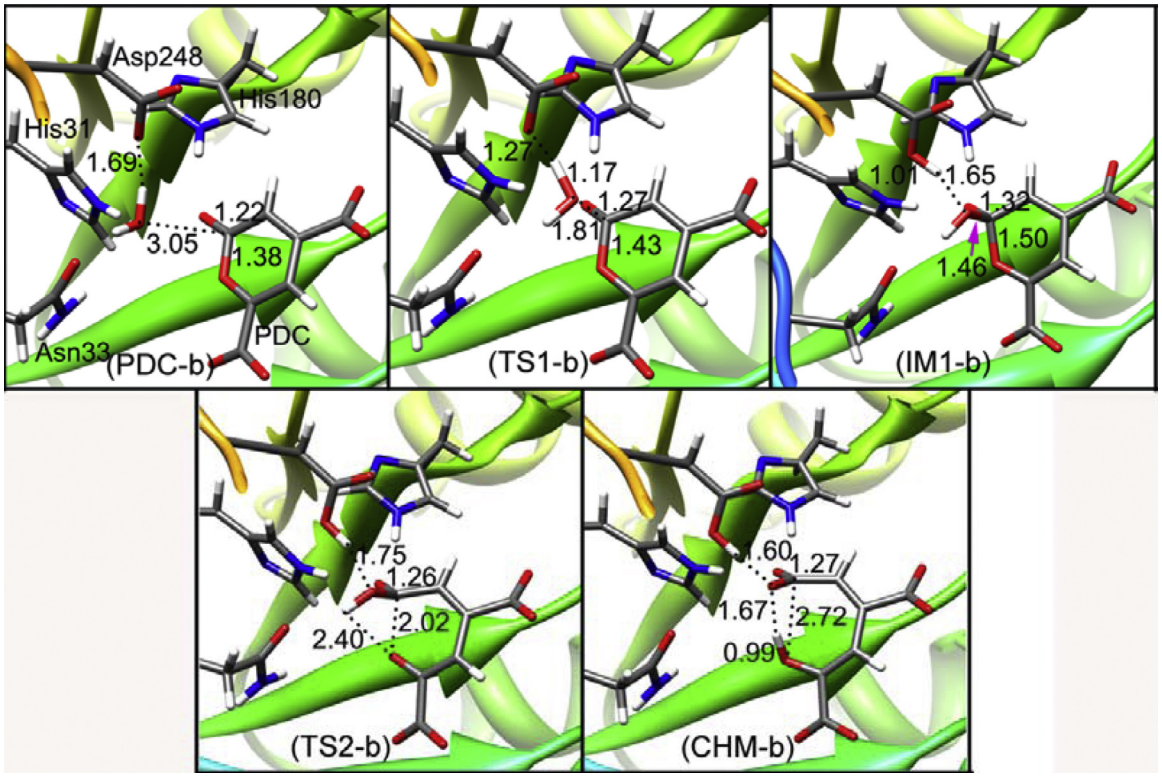

Fig. 7. Optimized geometries for H33N mutant. Distances are given in Å.

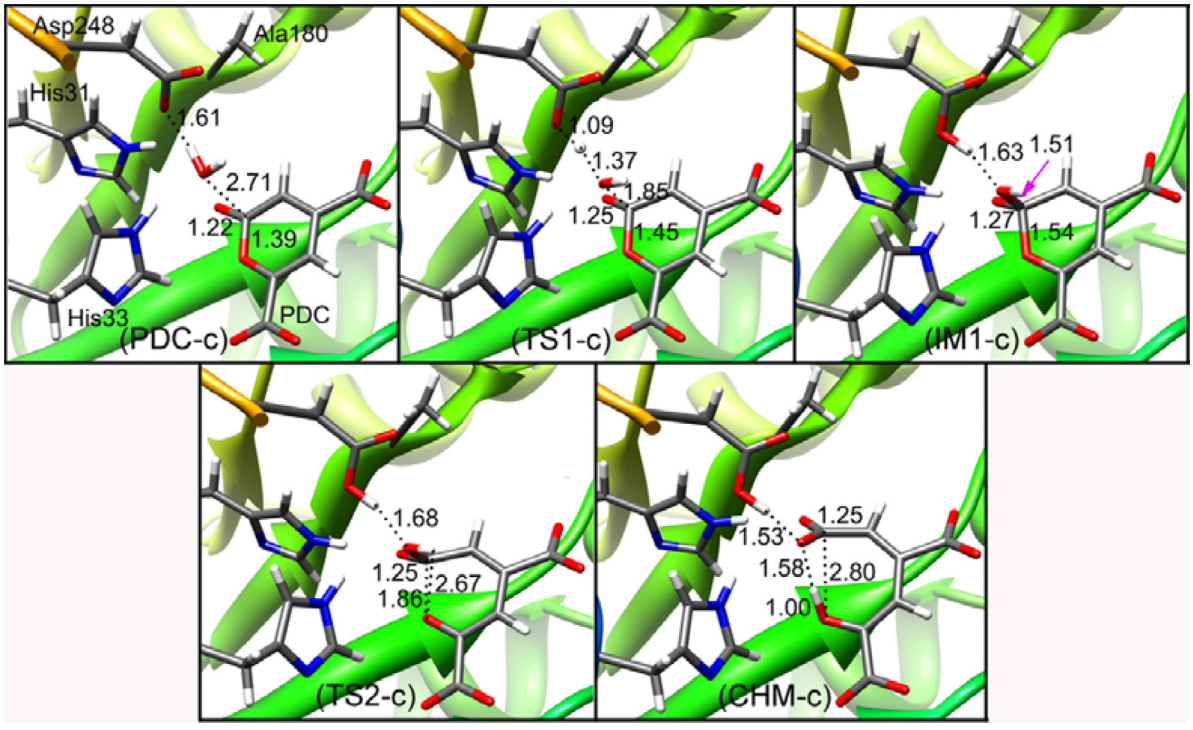

Fig. 8. Optimized geometries for H180A mutant. Distances are given in Å.

type enzyme (1.56 and 2.62 Å). The calculated energy barrier for the first step of H180A mutant is 13.7 kcal/mol, which is slightly higher than that of the wild type enzyme. The relative energy of intermediate IM1-c is 11.9 kcal/mol, which is 4.7 kcal/mol higher than IM1 in the wild type enzyme, indicating that His180 also has a function to stabilize the intermediate (IM1) by forming hydrogen bond. Similar to H31N and H33N mutant, the cleavage of C2—O1 bond is also coupled with the intramolecular proton transfer, corresponding to an energy barrier of 1.8 kcal/mol. For H180A mutant, the whole energy barrier is 13.7 kcal/mol, which is slightly lower than the estimated value of 16.5 kcal/mol calculated from the k_{cat} of 8.0 s^{-1}.

The superposition between H180A and the wild type enzyme is shown in Fig. S7. One can see that there is a slight structural change compared with the wild type enzyme.

4. Conclusion

In the present work, the detailed catalytic mechanism of LigI from *S. paucimobilis* has been studied by using a combined QM/MM method. Our calculation results suggest that, for the wild type enzyme, the whole catalytic reaction contains three elementary steps. The first step is the activation of the hydrolytic water molecule and the nucleophilic attack of the generated hydroxyl anion on the substrate, which proceeds in concerted manner, but the activation of the hydrolytic water molecule is prior to the nucleophilic attack. The second and third steps are the cleavage of C2—O1 bond of the lactone and an intramolecular proton transfer. The overall energy barrier energy of the catalytic reaction is about 14.0 kcal/mol, which is in consistent with the estimated free energy barrier of 14.2 kcal/mol. From the energy point of view, the enol form of the product (CHM) is the main product in the active site. Based on this, we presume that the isomerization of the two forms (CHM and OMA) occurs in solution, which is quite easy, but not in the active site. It is the pH value of the solution that determines the ratio of CHM and OMA. It should be noted that for the three mutated enzymes, the cleavage of C—O bond of the lactone is coupled with the proton transfer, and therefore, only two elementary steps are included in the hydrolysis of PDC.

Residue Asp248 acts as a general base to activate the hydrolytic water molecule. Other three residues His31, His33 and His180 do not directly participate in the chemical process, but they play assistant roles in activating the carbonyl group of the substrate and stabilizing the intermediates and transition states.

In general, our calculation results may provide useful information for understanding the chemical process occurred in the active site, and for illustrating the roles of pocket residues. The present study also provides useful help for studying the biodegradation polyesters of PDC [1,3,42].

Acknowledgements

This work was supported by the Natural Science Foundation of China (21173129, 21373125), the Research Award Foundation for outstanding young scientist of Shandong Province (BS2013SW028), and the Taishan Scholars Climbing Program of Shandong Province.

Appendix A. Supplementary data

Supplementary data associated with this article can be found, in the online version, at http://dx.doi.org/10.1016/j.jmgm.2015.06.011001

References

[1] M. Hishida, K. Shikinaka, Y. Katayama, S. Kajita, E. Masai, M. Nakamura, Y. Otsuka, S. Ohara, K. Shigehara, Polyesters of 2-pyrone-4,6-dicarboxylic acid (PDC) as bio-based plastics exhibiting strong adhering properties, Polym. J. 41 (2009) 297–302.
[2] M.E. Hobbs, V. Malashkevich, H.J. Williams, C. Xu, J.M. Sauder, S.K. Burley, S.C. Almo, F.M. Raushel, Structure and catalytic mechanism of LigI: insight into the amidohydrolase enzymes of cog3618 and lignin degradation, Biochemistry 51 (2012) 3497–3507.
[3] T. Michinobu, M. Bito, Y. Yamada, M. Tanimura, Y. Katayama, E. Masai, M. Nakamura, Y. Otsuka, S. Ohara, K. Shigehara, Fusible, elastic, and biodegradable polyesters of 2-pyrone-4,6-dicarboxylic acid (PDC), Polym. J. 41 (2009) 1111–1116.
[4] X. Peng, E. Masai, H. Kitayama, K. Harada, Y. Katayama, M. Fukuda, Characterization of the 5-carboxyvanillate decarboxylase gene and its role in lignin-related biphenyl catabolism in *Sphingomonas paucimobilis* SYK-6, Appl. Environ. Microbiol. 68 (2002) 4407–4415.
[5] M.E. Brown, M.C.Y. Chang, Exploring bacterial lignin degradation, Curr. Opin. Chem. Biol. 19 (2014) 1–7.
[6] I.C. Kuan, K.A. Johnson, M. Tien, Kinetic analysis of manganese peroxidase. The reaction with manganese complexes, J. Biol. Chem. 268 (1993) 20064–20070.
[7] S. Camarero, S. Sarkar, F.J. Ruiz-Duen˜as, M.J. Martínez, A.T. Martínez, Description of a versatile peroxidase involved in the natural degradation of lignin that has both manganese peroxidase and lignin peroxidase substrate interaction sites, J. Biol. Chem. 274 (1999) 10324–10330.
[8] P.J. Kersten, S. Dagley, J.W. Whittaker, D.M.J.D. Arciero, Lipscomb, 2-pyrone-4,6-dicarboxylic acid, a catabolite of gallic acids in *Pseudomonas* species, J. Bacteriol. 152 (1982) 1154–1162.
[9] M.E. Hobbs, M. Vetting, H.J. Williams, T. Narindoshvili, D.M. Kebodeaus, B. Hillerich, R.D. Seidel, S.C. Almo, F.M. Raushel, Discovery of an L-fucono-1,5-lactonase from cog3618 of the amidohydrolase superfamily, Biochemistry 52 (2013) 239–253.
[10] C.M. Seibert, F.M. Raushel, Structural and catalytic diversity within the amidohydrolase superfamily, Biochemistry 44 (2005) 6383–6391.
[11] M.E. Hobbs, H.J. Williams, B. Hillerich, S.C. Almo, F.M. Raushel, L-galactose metabolism in bacteroides vulgates from the human gut and microbiota, Biochemistry 53 (2014) 4661–4670.
[12] S.V. Ghodge, A.A. Fedorov, E.V. Fedorov, B. Hillerich, R. Seidel, S.C. Almo, F.M. Raushel, Structural and mechanistic characterization of L-histidinol phosphate phosphatase from the polymerase and histidinol phosphatase family of proteins, Biochemistry 52 (2013) 1101–1112.
[13] D.F. Xiang, P. Kolb, A.A. Fedorov, M.M. Meier, L.V. Fedorov, T.T. Nguyen, R. Sterner, S.C. Almo, B.K. Shoichet, F.M. Raushel, Functional annotation and three-dimensional structure of Dr0930 from *Deinococcus radiodurans*, a close relative of phosphotriesterase in the amidohydrolase superfamily, Biochemistry 48 (2009) 2237–2247.
[14] E. Masai, Y. Katayama, S. Nishikawa, M. Fukuda, Characterization of *Sphingomonas paucimobilis SYK-6* genes involved in degradation of lignin-related compounds, J. Ind. Microbiol. Biotechnol. 23 (1999) 364–373.
[15] E. Hara, K. Masai, Y. Miyauchi, Characterization of the 4-carboxy-4-hydroxy-2-oxoadipate aldolase gene and operon structure of the protocatechuate 4,5-cleavage pathway genes in *Sphingomonas paucimobilis* SYK-6, J. Bacteriol. 185 (2003) 41–50.
[16] E. Masai, K. Momose, H. Hara, S. Nishikawa, Y. Katayama, M. Fukuda, Genetic and biochemical characterization of 4-carboxy-2-hydroxymuconate-6-semialdehyde dehydrogenase and its role in the protocatechuate 4,5-cleavage pathway in *Sphingomonas paucimobilis* SYK-6, J. Bacteriol. 182 (2000) 6651–6658.
[17] D. Dutta, S. Mishra, The structural and energetic aspects of substrate binding and the mechanism of action of the DapE-encoded *N*-succinyl-l, L-diaminopimeLic acid desuccinylase (DapE) investigated using a hybrid QM/MM method, Phys. Chem. Chem. Phys. 16 (2014) 26348–26358.
[18] A.R. Calixto, N.F. Brás, P.A. Fernandes, M.J. Ramos, Reaction mechanism of human renin studied by quantum mechanics/molecular mechanics (QM/MM) calculations, ACS Catal. 4 (2014) 3869–3876.
[19] J. Kim, P.C. Tsai, S.L. Chen, F. Himo, S.C. Almo, F.M. Raushel, Structure of diethyl phosphate bound to the binuclear metal center of phosphotriesterase, Biochemistry 47 (2008) 9497–9504.
[20] D. Li, C. Liu, J. Lin, Theoretical study of the mechanism of protein arginine deiminase 4 (PAD4) inhibition by F-amidine, J. Mol. Graph. Model. 55 (2015) 25–32.
[21] J. Wang, R. Zhang, R. Liu, Y. Liu, Investigation of the rescue mechanism catalyzed by a nucleophile mutant of rice BGlu1, J. Mol. Graph. Model. 54 (2014) 100–106.
[22] H. Su, L. Dong, Y. Liu, A QM/MM study of the catalytic mechanism of α-1, 4-glucan lyase from the red seaweed Gracilariopsis lemaneiformis, RSC Adv. 4 (2014) 54398–54408.
[23] X. Sheng, J. Gao, Y. Liu, C. Liu, Theoretical study on the proton shuttle mechanism of saccharopine dehydrogenase, J. Mol. Graph. Model. 44 (2013) 17–25.
[24] G. Ma, L. Dong, Y. Liu, Insights into the catalytic mechanism of dTDP-glucose,6-dehydratase from quantum mechanics/molecular mechanics simulations, RSC Adv. 4 (2014) 35449–35458, 4.
[25] W. Humphrey, A. Dalke, K. Schulten, VMD: visual molecular dynamics, J. Mol. Graphics 14 (1996) 33–38.
[26] M.H.M. Olsson, C.R. Søndergard, M. Rostkowski, J.H. Jensen, PROPKA3: consistent treatment of internal and surface residues in empirical pK_a predictions, J. Chem. Theory Comput. 7 (2011) 525–537.
[27] B.R. Brooks, R.E. Bruccoleri, B.D. Olafson, D.J. States, S. Swaminathan, M. Karplus, CHARMM: a program for macromolecular energy, minimization, and dynamics calculations, J. Comput. Chem. 4 (1983) 187–217.
[28] A.D. MacKerell Jr., D. Bashford, M. Bellott, R.L. Dunbrack Jr., J.D. Evanseck, M.J. Field, S. Fischer, J. Gao, H. Guo, S. Ha, D. Joseph-McCarthy, L. Kuchnir, K. Kuczera, F.T.K. Lau, C. Mattos, S. Michnick, T. Ngo, D.T. Nguyen, B. Prodhom, W.E. Reiher III, B. Roux, M. Schlenkrich, J.C. Smith, R. Stote, J. Straub, M. Watanabe, J. Wiórkiewicz-Kuczera, D. Yin, M. Karplus, All-atom empirical potential for molecular modeling and dynamics studies of proteins, J. Phys. Chem. B. 102 (1998) 3586–3616.
[29] P. Sherwood, A.H. de Vries, M.F. Guest, G. Schreckenbach, C.R.A. Catlow, S.A. French, A.A. Sokol, S.T. Bromley, W. Thiel, A.J. Turner, S. Billeter, F. Terstegen, S. Thiel, J. Kendrick, S.C. Rogers, J. Casci, M. Watson, F. King, E. Karlsen, M. Sjøvoll, A. Fahmi, A. Schäfer, C. Lennartz, QUASI: a general purpose

implementation of the QM/MM approach and its application to problems in catalysis, J. Mol. Struct.: THEOCHEM 632 (2003) 1–28.
[30] R. Ahlrichs, M. Bär, M. Häser, H. Horn, C. Kälmel, Electronic structure calculations on workstation computers: the program system turbomole, Chem. Phys. Lett. 162 (1989) 165–169.
[31] W. Smith, T.R. Forester, DL_POLY_2. 0: a general-purpose parallel molecular dynamics simulation package, J. Mol. Graphics 14 (1996) 136–141.
[32] S.R. Billeter, A.J. Turner, W. Thiel, Linear scaling geometry optimisation and transition state search in hybrid delocalized internal coordinates, Phys. Chem. Chem. Phys. 2 (2000) 2177–2186.
[33] A.H. de Vries, P. Sherwood, S.J. Collins, A.M. Rigby, M. Rigutto, G.J. Kramer, Zeolite structure andreactivity by combined quantum-chemical-classical calculations, J. Phys. Chem. B. 103 (1999) 6133–6141.
[34] M.J. Field, P.A. Bash, M. Karplus, A combined quantum mechanical and molecular mechanical potential for molecular dynamics simulations, J. Comput. Chem. 11 (1990) 700–733.
[35] J. Nocedal, Updating quasi-Newton matrices with limited storage, Math. Comput. 35 (1980) 773–782.
[36] D.C. Liu, J. Nocedal, On the limited memory BFGS method for large scale optimization, Math. Program. 45 (1989) 503–528.
[37] A. Banerjee, N. Adams, J. Simons, R. Shepard, Search for stationary points on surfaces, J. Phys. Chem. 89 (1985) 52–57.
[38] J. Baker, An algorithm for the location of transition states, J. Comput. Chem. 7 (1986) 385–395.
[39] D. Quiñonero, C. Garau, A. Frontera, P. Ballester, A. Costa, P.M. Deyà, Structure and binding energy of anion-π and cation-π complexes: a comparison of MP2, RI-MP2, DFT, and DF-DFT methods, J. Phys. Chem. A 109 (2005) 4632–4637.
[40] S. Grimme, Semiempirical GGA-type density functional constructed with a long-range dispersion correction, J. Comput. Chem. 27 (2006) 1787–1799.
[41] W. Gao, H. Feng, X. Xuan, L. Chen, The assessment and application of an approach to noncovalent interactions: the energy decomposition analysis (EDA) in combination with DFT of revised dispersion correction (DFT-D3) with slater-type orbital (STO) basis set, J. Mol. Model. 18 (2012) 4577–4589.
[42] M. Michinobu, M. Hishida, Y. Sato, E. Katayama, M. Masai, Y. Nakamura, S. Ohara, K. Shigehara, Polyesters of 2-pyrone-4,6-dicarboxylic acid (PDC) obtained from a metabolic intermediate of lignin, Polym. J. 40 (2008) 68–75.
[43] C.L. Brooks, A. Brünger, M. Karplus, Active site dynamics in protein molecules: a stochastic boundary molecular–dynamics approach, Biopolymers 24 (1985) 843–865.
[44] P. Sherwood, A.H. de Vries, M.F. Guest, et al., QUASI: a general purpose implementation of the QM/MM approach and its application to problems in catalysis, J. Mol. Struct.: THEOCHEM 632 (2003) 1–28.